CHAPTER

Expansion microscopy of the mitotic spindle

12

Ivana Ponjavić*, Kruno Vukušić, and Iva M. Tolić
Division of Molecular Biology, Ruđer Bošković Institute, Zagreb, Croatia
**Corresponding author: e-mail address: iponjav@irb.hr*

Chapter outline

Methods in Cell Biology, Volume 161, ISSN 0091-679X, https://doi.org/10.1016/bs.mcb.2020.04.014

Abstract

The mitotic spindle is a dynamic and complex cellular structure made of microtubules and associated proteins. Although the general localization of most proteins has been identified, the arrangement of the microtubules in the mitotic spindle and precise localization of various proteins are still under intensive research. However, techniques used previously to decipher such puzzles are resolution limited or require complex microscopy systems. On the other hand, expansion microscopy is a novel super-resolution microscopy technique that uses physical expansion of fixed specimens to allow features closer than the diffraction limit of light (~250 nm) to become resolvable in the expanded specimen on a conventional confocal microscope. This chapter focuses on expansion microscopy of the mitotic spindle, specifically using tubulin labeling to visualize all microtubule subpopulations within the spindle. Furthermore, we discuss a protocol for expansion of GFP-tagged proteins, such as protein regulator of cytokinesis 1 (PRC1). We also discuss various approaches for image analysis pointing out main advantages of expansion microscopy when compared to previously used techniques. This approach is currently used in our laboratory to study the architecture of the microtubules in the mitotic spindle after perturbations of various proteins important for the structural and dynamical properties of the mitotic spindle.

1 Introduction

During cell division, a fundamental process in all living organisms, the genetic material is equally divided into two newly formed daughter cells. To ensure accurate segregation of chromosomes, the cell forms the mitotic spindle—a dynamic and robust micro-machine assembled of microtubules and a variety of associated proteins (Forth & Kapoor, 2017; Maiato, Gomes, Sousa, & Barisic, 2017; Pavin & Tolić, 2016; Prosser & Pelletier, 2017; Vukušić, Buđa, & Tolić, 2019). To get insight into the localization of different proteins that are essential to the mitotic spindle and its architecture, optical imaging techniques are used. However, the optical diffraction limit precludes conventional optical imaging approaches from resolving structures with feature sizes smaller than ~250 nm (Born et al., 1999).

Recent innovations have led to the development of three main commercially available options for super-resolution microscopy that effectively break the diffraction limit: structured illumination microscopy (SIM) (Gustafsson, 2000), stochastic optical reconstruction microscopy (STORM)/photoactivation localization microscopy (PALM) (Betzig et al., 2006; Rust, Bates, & Zhuang, 2006), and stimulated emission depletion microscopy (STED) (Klar, Jakobs, Dyba, Egner, & Hell, 2000). Between these super-resolution techniques, there are many differences which then influence how suited an approach is to study a specific question in biology (Coelho, Maghelli, & Tolić-Nørrelykke, 2013; Thorley, Pike, & Rappoport, 2014). One thing that these super-resolution methods have in common is that they all require additional software, specific parts of the microscope or a completely new microscope.

Expansion microscopy (ExM) is a newly developed super-resolution microscopy technique that uses physical expansion of a fixed specimen to allow features closer than the diffraction limit of light to become resolvable in the expanded specimen (Chen, Tillberg, & Boyden, 2015). ExM is developing rapidly (Asano et al., 2018; Chang et al., 2017; Chozinski et al., 2016; Geertsema & Ewers, 2016; Zhang et al., 2016; Zhao et al., 2017), allowing now for the use of conventional immunofluorescence labeling approaches on both proteins and RNAs (Chen et al., 2016; Chozinski et al., 2016; Tillberg et al., 2016), and it has been tested on different samples from pathological preparations (Asano et al., 2018; Zhao et al., 2017) to brain sections (Zhang et al., 2016). It is a technique that circumvents the diffraction limit by embedding fluorophores into a swellable polymer that is physically expanded and reaches a linear expansion factor of 4.5 and a volumetric expansion factor of 90 (Asano et al., 2018), to enable super-resolution microscopy with conventional diffraction limited microscopes. The main advantage of ExM is its availability to scientists who have access to a conventional microscope, without need for a new software or special parts for the microscope (Gao, Asano, & Boyden, 2017). An approach to further improve the resolution of STED microscopy in 3D by combining it with ExM has recently been introduced (Gambarotto et al., 2019; Gao et al., 2018). Moreover, the expansion factor has been enhanced from approximately fourfold to tenfold using standard expansion microscopy protocols (Truckenbrodt et al., 2018; Truckenbrodt, Sommer, Rizzoli, & Danzl, 2019) and up to 53× expansion when using iterative expansion microscopy protocols (Chang et al., 2017).

Basic principles of ExM are as follows: fixed proteins within the cell, including both biomolecules and introduced labels, are covalently anchored to a hydrogel matrix with commercially available small molecules such as Acryloyl-X SE (Ac-X), that binds to primary amine groups on proteins (Tillberg et al., 2016). There are also alternatives to Ac-X such as glutaraldehyde (GLA), where GLA is linked to the acrylamide polymer through either covalent or topological mechanisms (Chozinski et al., 2016) (Fig. 1A) or formaldehyde/acrylamide mix (PFA/AA), where with increased AA concentration, methylols formed by the protein-formaldehyde reaction preferentially react with excess AA monomers, effectively reducing inter-protein crosslinking while maximally tethering individual proteins to an expandable hydrogel mesh (Gambarotto et al., 2019; Ku et al., 2016). These complexes are

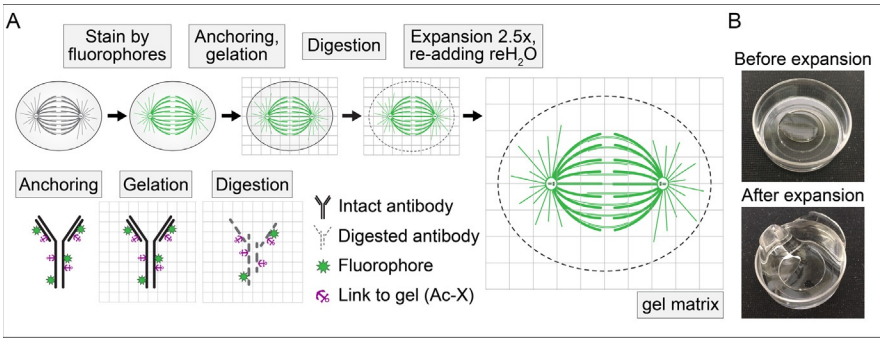

FIG. 1

Schematic workflow of expansion microscopy of the mitotic spindle highlighting key steps of the protocol. (A) After conventional immunostaining with fluorophore-conjugated antibodies, anchoring agents are used to link the entire sample by polymer-linking groups to the polymer matrix. After gelation of the polymer, the sample is digested by Proteinase-K treatment and later isotropically expanded by subsequent addition of ddH_2O. The bottom part highlights the key steps of the protocol regarding protein-conjugated antibody.
(B) Photographs of a gel in a dish, before and after expansion with ddH_2O.

Figure is adapted from Chozinski et al. (2016).

then incorporated into the hydrogel polymer during the process of polymerization that forms a dense polyelectrolyte hydrogel (Wassie, Zhao, & Boyden, 2019) (Fig. 1A). An enzymatic overnight digestion using proteinase-K (ProK) mechanically disrupts and homogenizes the embedded sample, allowing the isotropic expansion by swelling resulting from water diffusing within the gel through osmotic force, while most fluorophores are sufficiently resistant to this overnight proteolysis (Asano et al., 2018) (Fig. 1A and B).

2 Rationale

Mitotic spindle is a very dynamic and dense structure and it is often hard to capture the proper localization of proteins that are essential for the spindle, especially with live microscopy, and that is why we need to rely on fixed specimens and immunofluorescence to study the architecture of the spindle. Today, we can use ExM as an improved version of the immunofluorescence protocol (Chozinski et al., 2016) and get super-resolution images of essential proteins in the mitotic spindle. Tubulin is perhaps one of the most intriguing proteins to visualize in the spindle using ExM and the first example of this approach was published in a method paper using tubulin immunostaining of PTK1 cells (Chozinski et al., 2016). Tubulin in the mitotic spindles of zebrafish (Freifeld et al., 2017) and tubulin-GFP in early metaphase-I spindle of mouse oocytes (So et al., 2019) has also been expanded. Except anti-alpha tubulin

and tubulin-GFP, kinetochore protein Hec1 (Chozinski et al., 2016), tetrameric kinesin KIF25 (Decarreau et al., 2017), GFP-Spindly and mCherry-tubulin (Sacristan et al., 2018) have been expanded recently as well in mammalian systems.

Here, we describe the optimized protocols for ExM of human mitotic spindles immunostained for tubulin, and centromere protein Hec1, as well as protocols for ExM of mitotic spindles labeled with endogenously tagged microtubule-associated protein PRC1, which required adaptations of the original protocol. One of the most useful parts of our ExM protocol is the protocol for tubulin immunostaining which, even when used without the expansion, gives plenty of information about the architecture of the spindle. However, we illustrate the greater power of ExM protocols used to study the mitotic spindle structure, when compared to immunofluorescence without expansion, which enable better structural characterization of defined structures within the mitotic spindle, such as bridging fibers which link two sister k-fibers (Kajtez et al., 2016). Moreover, applied protocols allow superior resolution of microtubule bundle distribution in different populations of microtubules, and provide a better insight into the localization of specific proteins within the spindle.

3 Cons of expansion microscopy

One of the limitations of the ExM is the reduced fluorescence signal after expansion (Chen et al., 2015; Tillberg et al., 2016). This could be caused by (i) fluorophore damage during gel polymerization, (ii) incompatibility of some dyes with the digestion step, and (iii) dilution of dyes during the expansion step. Some fluorophores are completely incompatible with ExM (Chen et al., 2015; Tillberg et al., 2016; Truckenbrodt et al., 2018), meaning they are destroyed in digestion. In order to reduce the loss of fluorescence, the post-expansion immunostainings can be applied, in which either only the secondary antibody or both the secondary and the primary antibodies are applied after expansion (Wang et al., 2018). As the sample expansion occurs in all three dimensions, the thickness of the sample can cause issues with imaging thick samples and optical aberrations (Gao et al., 2018). Although the expanded gel is 99% clear water, most high-magnification objectives have a shorter working distance than what is needed for these types of samples. Finally, since the presented protocol of the ExM of the mitotic spindle requires fixation, it is only compatible with fixed samples.

4 Materials and reagents

4.1 Biological materials

This protocol is adapted for human cell cultures (see Section 5.1.), for other types of biological materials consult other sources (Asano et al., 2018).

4.2 Reagents

- 6-((Acryloyl)amino)hexanoic Acid, Succinimidyl ester (Acryloyl-X, SE; Thermo Fisher Scientific, cat. no. A-20770)
- NaCl (Sigma-Aldrich, cat. no. S7653)
- KCl (Sigma-Aldrich, cat. no. P9333)
- Dimethyl sulfoxide (DMSO; Thermo Fisher Scientific, cat. no. D12345)
- $MgCl_2$ (Sigma Aldrich, cat. no. M8266)
- Borohydride (Sigma Aldrich, cat. no. 213462)
- Sodium acrylate (SA; Sigma-Aldrich, cat. no. 408220)

  Note: Sodium acrylate is dangerous to the aquatic environment. Wear appropriate protective equipment and work under a fume hood. We recommend checking the purity of SA whenever a new batch is opened, by making a 0.38 g/mL stock and evaluating if the solution is colorless. If the solution has a strong yellow tint, discard the batch and use a newly opened one, as polymerization is strongly negatively affected by use of impure SA. We recommend storing SA at −20 °C in a desiccated environment to preserve stability, and to regularly repeat the test until the batch is used up.
- RO-3360 inhibitor (Sigma-Aldrich, cat. no. 217699)
- MG-132 inhibitor (Sigma-Aldrich, cat. no. 474790)
- PIPES (Sigma, cat. no. P6757-500G)
- EDTA (Sigma-Aldrich, cat. No. EDS)
- Triton-X-100 (Sigma-Aldrich, cat. no. 93426)

  Note: Triton-X-100 is corrosive and acutely toxic to the aquatic environment. Wear protective equipment and work under a fume hood.
- Paraformaldehyde 4% (PFA, Santa Cruz Biotechnology, sc-281692)

  Note: Paraformaldehyde is a carcinogen. Wear protective equipment and work under a fume hood.
- Glutaraldehyde 50% (GLA, Sigma-Aldrich, cat. no. G7651)

  Note: Glutaraldehyde is a carcinogen. Wear protective equipment and work under a fume hood.
- Phosphate-buffered saline (PBS, Dulbecco, cat. no. L 182-50)
- Immunopure Normal Goat Serum (NGS, Thermo-Fisher Scientific, cat. no. 31872)

  Note: Be careful when choosing the blocking buffer since it precludes the usage of specific antibodies from the animal from which the serum was isolated, in this case goat made antibodies could not be used.
- Primary antibodies used here: rat anti-alpha Tubulin YL1/2 (MA1-80017, Thermo Fisher Scientific).
- Secondary antibodies used here: donkey anti-rat Alexa Fluor 594 (Abcam, cat. no. ab150156).

  Note: Secondary antibody should match the primary antibody in a way that the secondary antibody is raised against the host species used to generate the primary antibody. For instance, if you use a primary antibody raised in rat, as in

this case, you will need an anti-rat secondary antibody raised in a host species other than rat (e.g., donkey anti-rat secondary).
- Silicone rhodamine (SiR)-DNA (Spirochrome, cat. no. sc007)
- 40% Acrylamide/Bis-acrylamide solution 29:1 (Bio-Rad, cat. no. 161–0146)
- Ammonium persulfate (APS, Bio-Rad, cat. no. 161–0700)
- *N*,*N*,*N*′,*N*′-tetramethylethane-1,2-diamine (TEMED, Sigma-Aldrich, cat. no. T7024)

  Note: *N*,*N*,*N*′,*N*′-tetramethylethane-1,2-diamine is flammable and corrosive. Wear protective equipment and work under a fume hood.
- Tris(hydroxymethyl)aminomethane (TRIS, Carl Roth GmbH + Co. KG, art. no. 4855.2)
- Guanidine-HCl (Sigma-Aldrich, cat. no. G45059)
- Proteinase-K (Sigma-Aldrich, cat. no. P4850)

4.3 Reagent setup

4.3.1 PEM buffer

To make PEM buffer, prepare 0.1 M PIPES pH 7.1, 1 mM EDTA, 1 mM $MgCl_2$ and 0.5% Triton-X-100 in double-distilled water (ddH_2O) (made from stock of 10% Triton-X-100), and adjust the pH to 6.9. This solution can be stored at −20 °C for several weeks.

4.3.2 Fixative

To make a 3.2% paraformaldehyde and 0.1% glutaraldehyde fixative solution, add 40 mL of 4% paraformaldehyde and 0.1 mL of 50% glutaraldehyde in 9.9 mL of previously prepared PEM buffer. This solution can be stored at −20 °C for several weeks.

4.3.3 Blocking/permeabilization buffer

Blocking/permeabilization solution is PBS + 2.5% (wt/vol) NGS + 0.1% (vol/vol) Triton X-100. Prepare the blocking/permeabilization solution fresh each time.

4.3.4 Monomer solution

To make 2 mL of monomer solution for gelation, add 480 µL of 38% sodium acrylate, 125 µL of 40% Acrylamide/Bis-acrylamide Solution, 850 µL of 29.2% sodium chloride, 210 µL of 10 × PBS and 335 µL of ddH_2O. Prepare the monomer solution fresh each time.

4.3.5 Anchoring reagent stock

To make anchoring the reagent stock, dissolve Acryloyl-X in anhydrous DMSO to a concentration of 10 mg/mL. When using glutaraldehyde reagent, dilute 50% GLA to 0.25% solution in water. Store these stocks at −20 °C in a desiccated environment.

4.3.6 Anchoring buffer

The anchoring buffer is PBS at pH 7.0–7.4. PBS can be stored at room temperature for several months.

4.3.7 Digestion buffer

To make the digestion buffer, prepare 50 mM Tris pH 8.0, 1 mM EDTA, 0.5% Triton X-100 and 0.8 M guanidine-HCl in ddH_2O. Add proteinase-K at a concentration of 8 U/mL to the digestion buffer immediately before use. The buffer can be stored (without proteinase-K) at −20 °C for at least 6 months.

5 Protocols

5.1 Cell culture

Human hTERT-RPE-1 stable cell line expressing CENP-A-GFP and centrin1-GFP were grown in flasks in Dulbecco's modified Eagle's medium (DMEM) (1 g/L D-glucose, L-glutamine, pyruvate) (Lonza, Basel, Switzerland) supplemented with 10% of heat-inactivated fetal bovine serum (Sigma-Aldrich, St. Louis, MO, USA), 100 I.U./mL penicillin and 100 mg/mL streptomycin solution (Lonza). Human U2OS stable cell lines expressing CENP-A-GFP and HeLa-Kyoto BAC line stably expressing PRC1-GFP were grown in the same DMEM medium, with addition of 50 mg/mL geneticin (Life Technologies, Waltham, MA, USA). Cells were passaged after reaching 100% confluence. Cells were kept at 37 °C and 5% CO_2 in a humidified incubator.

A day prior to imaging, cells were seeded on 35 mm glass coverslip uncoated dishes with 0.17 mm glass thickness (MatTek Life Sciences, Ashland, MA, USA) in 1.5 mL DMEM medium with appropriate supplements. Note that good seeding of the cells is a critical step if you study mitosis, because one must maximize the number of mitotic cells in the dish at the time of fixation, and this is observed at confluences above 80%. The protocol we optimized and followed, when seeding the cells 1 day before fixation, was to do a 1/5 dilution of the 80–100% confluent cell culture grown in a flask, then add the 400 µL of the diluted cells into 35 mm glass coverslip dishes, corresponding to $\sim 0.4 \times 10^6$ cells in each dish.

5.2 Cell synchronization

The fraction of cells in mitosis in a population of cells is known as the mitotic index (MI). In rapidly-proliferating cell populations the MI can be as high as 10%, and in slowly proliferating populations the MI can be extremely low, down to 0.1% (Hendry & Scott, 1987), which means that even in the sample of rapidly proliferating cells, the fraction of cells in mitosis is relatively low. When expanding the sample, the space between the cells is also expanding and that leads to a decreased possibility of finding mitotic spindles in the expanded sample. For this reason, cutting the gel into smaller pieces is recommended when studying rare phenomena by ExM

(Asano et al., 2018). To increase the number of mitotic spindles, especially in metaphase, two inhibitors were used. Inhibitor RO-3360 is a selective small-molecule inhibitor of Cyclin-dependent kinase-1 (CDK1) that reversibly arrests human cells at the G_2/M border of the cell cycle allowing for effective cell synchronization in early mitosis (Vassilev et al., 2006). 24 h after the addition of the inhibitor RO-3360, the cell medium was removed and the cells were washed three times with 1 mL of sterile 1% PBS buffer. After the washout, a new, warm cell medium was added and the cells were stored in the incubator. After a period of 30 min up to 1 h, depending on the cell line, a large number of cells that were blocked at the G_2/M border of the cell cycle, synchronously enter mitosis. Usually, around 40% of Hela or U2OS cells entered mitosis approximately 30 min after washout of RO-3360, while RPE1 cells required longer incubation times after washout, up to 1 h. If fixed at this stage, the population is enriched in mitotic spindles found mostly in prophase/prometaphase (Fig. 2, left).

To get more spindles in metaphase, MG-132 inhibitor was used. MG-132 is a proteasome inhibitor, and due to its low cost and the rapid reversibility of its action, it is the first choice to block proteasome function, required for the last step in ubiquitin-mediated degradation of securin, a hallmark of the anaphase onset (Kisselev & Goldberg, 2001; Thornton & Toczyski, 2003). MG-132 inhibitor was added 30–60 min after RO-3360 washout and was left to incubate for 15–20 min without washing it out afterwards. After that, the population of cells in the sample was enriched with mitotic spindles in metaphase (Fig. 2, middle) and the cells were ready to be fixed.

For experiments in which post-metaphase spindles were required (Fig. 2, right), no synchronization protocol was followed, and in that situation good seeding was critical (see Cell culture section).

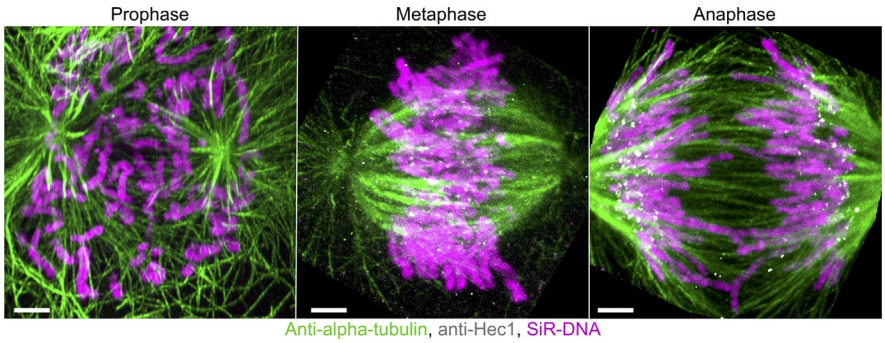

FIG. 2

Expansion microscopy of the mitotic spindle in various phases of mitosis. Maximum z-projections of RPE-1 cells immunostained for anti-alpha tubulin (green), anti-Hec1 (white) and labeled with 100 nM SiR-DNA (magenta) and expanded in different phases of mitosis as indicated. Scale bars, 5 μm.

5.3 Choosing the right fixative

Choosing the right fixative is very important because it can determine the efficiency of antibody binding to its substrate, since some fixatives tend to change the epitope of the target protein thereby reducing or diminishing the expected signal. Generally, we noticed that 3.2% PFA/0.1% GLA fixative is best suited for fixation of alpha-tubulin, either by fixing fluorescently tagged tubulin or unlabeled cells later stained with anti-alpha tubulin monoclonal antibody YL1/2 (see Section 4.2). However, this fixative is not suited for staining most microtubule-associated proteins, such as PRC1, because PFA reduces the signal of PRC1 labeled with fluorescent proteins on the mitotic spindle, and allows observation of PRC1 only in telophase cells. Moreover, when unlabeled cells are fixed using this protocol, PRC1 antibody does not bind to its epitope on the PRC1. We also noticed that the signal after labeling centromere proteins with antibodies, such as HEC1, is also weakened after usage of this fixative, similar to Chozinski et al. (2016).

Alternatively, cold-methanol fixation could be used but it carries additional problems. Usage of cold methanol tends to destroy unstable fractions of microtubules, destroying both astral microtubules and unstable fractions of interpolar microtubules (Busson, Dujardin, Moreau, Dompierre, & De Mey, 1998). Moreover, it tends to dissolve membrane lipids, preventing staining of the membrane components. Generally the signal-to-noise ratio obtained by methanol fixation is much smaller when compared with PFA/GLA fixation (Schnell, Dijk, Sjollema, & Giepmans, 2012). Furthermore, methanol sometimes causes shrinkage of the mitotic spindle, and the whole cell, sometimes just in one dimension, making results less reproducible and harder to interpret (Schnell et al., 2012).

Other fixation methods were also tested: 100% methanol fixation, 4% paraformaldehyde fixation, 4% paraformaldehyde and 0.1% glutaraldehyde in PEM buffer followed by 100% methanol fixation, 0.1% glutaraldehyde in PEM fixation and 3.2% paraformaldehyde in PEM fixation. None of them showed satisfying results regarding immunofluorescence of anti-tubulin and its subsequent expansion. For example, fixations that include 100% cold-methanol often reduced the length and width of the spindles. However, methanol has to be used to preserve microtubule-associated proteins, i.e., the ability of antibodies to bind to them (see below).

5.4 Choosing the right antibody

During pre-expansion staining, in the presence of GLA or AC-X, most fluorescent proteins and dyes are compatible with digestion protocol using ProK, that is, there is >50% fluorescence retention after digestion (Chozinski et al., 2016; Tillberg et al., 2016), except cyanine-family dyes (such as Alexa 647 or Cy5) that are degraded during the proteinase step. Therefore, for pre-expansion staining it is recommended to use Atto647N if a far-red dye is required. Regarding fluorescent proteins, GFP-like fluorescent proteins are mostly protease-resistant and can survive the ExM process well, with >50% fluorescence retention), but non-GFP-like fluorescent proteins such

as infrared proteins based on bacteriophytochrome are easily destroyed by the proteinase step (R. Gao et al., 2017). In this protocol, we used Alexa 488 and Alexa 594 secondary antibodies and GFP-labeled PRC1 protein.

5.5 Protocol for expansion microscopy of tubulin in the spindle

5.5.1 Day 1

Cytoskeletal buffer, fixation, reduction

1. Wash Previously Synchronized Cells (See Section 5.2), in 35 Mm Glass Coverslip Uncoated Dishes with 0.17 Mm (#1.5 Coverglass) Glass Thickness, with 1 mL of the PEM Buffer for 1 S

   Note: Fixation should be performed almost synchronously with addition of the PEM buffer because PEM contains Triton-X detergent and usage of such compounds on living cells causes an immediate burst of the large part of the cell membrane. This improves the signal-to-noise ratio by lowering the non-specific anchorage of antibodies to the components of the cytoplasm but a large fraction of cells can detach from the dish if PEM is left without fixative for more than a few seconds. In that regard, this step could be skipped during the initial tests of the protocol.
2. Immediately fix with 1 mL of the solution containing 3.2% PFA and 0.1% GLA in PEM for 10 min.
3. Wash cells in 1 mL of the 1% PBS buffer three times for 5 min each.
4. Incubate the sample in 1 mL of the 10 mM aqueous solution of sodium borohydride to reduce the aldehyde groups.

   Note: Washout with sodium borohydride reduces autofluorescence of glutaraldehyde which could otherwise interfere with the signal of fluorophores. Borohydride solution should be prepared fresh every time.
5. Wash cells in 1 mL of the 1% PBS buffer 3 times for 5 Min each

Blocking and permeabilization and incubation with primary antibody

6. Add 1 mL of the blocking/permeabilization buffer (PBS with 1% NGS and 0.5% Triton X-100) for 45 min to additionally permeabilize cells and remove nonspecific binding of antibody to the surface.
7. Incubate the sample in primary antibodies diluted in 1 mL of the blocking/permeabilization buffer, overnight at 4 °C on the orbital shaker. Use a humid chamber (we put a wet piece of tissue paper in the petri dish) to reduce the evaporation of the sample solution.

   Note: For start, final concentration of the antibody should be adjusted according to manufacturer's protocols, but it can be lowered or increased depending on the success of the expansion protocol. Manufacturer of our anti-alpha tubulin monoclonal primary antibody YL1/2 recommended 1:200–1:500 dilution and we used 1:500 dilution since we did not experience too much fluorophore loss following the digestion step (see below). Also, if needed, the incubation time of the primary antibody could be reduced or increased.

5.5.2 Day 2

Incubation with secondary antibody

8. Wash cells in 1 mL of the 1% PBS buffer three times for 5 min each. From this moment on, cover the petri dish with aluminum foil to prevent the loss of secondary antibody fluorescence.
9. Incubate in secondary antibody diluted in blocking/permeabilization buffer for 45 min on room temperature on orbital shaker.
10. Wash cells in 1 mL of the 1% PBS buffer three times for 5 min each, at room temperature.

Chromosome staining and quality control

11. For visualization of chromosomes, add 1 mL of the 50–100 nM solution of SiR–DNA or 1 mL of the 1 μg/mL solution of DAPI and incubate for 15–20 min, in case you need to image the cells before expansion. This is needed to later calculate the expansion factor or to observe the mitotic spindles and quality of their staining at this stage, since this corresponds to the end of a classic immunofluorescence protocol.

    Note: The quality of the immunofluorescence protocol will greatly determine the quality of the expansion signal itself, since from this moment in the protocol, the signal intensity of the fluorophore will drop after performing the subsequent steps and thus a good signal at the end of immunofluorescence is crucial for informative expansion.

Anchoring

12. Dilute the Acryloyl-X 1:100 (vol/vol) to 0.1 mg/mL in PBS (pH 7.0–7.4) and add it on the sample. Incubate for at least 6 h or overnight at room temperature. If using GLA anchoring, add 0.25% GLA on the sample and incubate for 10 min at room temperature.

    Note: Anchoring step is essential for integrating the sample into the gel matrix and the final ExM result depends greatly on this step.
13. Wash cells in 1 mL of the 1% PBS buffer for 5 Min

Gelation

14. Mix the previously prepared and cooled monomer solution on ice (see Section 4.3) with 0.2% solution of APS, 0.2% solution of TEMED and water. Add 200–400 μL to the sample in the dish and incubate the sample at 37 °C for 30 min.

    Note: It is important to work quickly in this step. After adding TEMED and APS, the polymerization reaction starts in a few seconds, so it is best to add the gelation solution to the sample in less than a minute after preparing it. It is imperative to bring the gelation solution to 0 °C for this step, as the addition of APS will otherwise initiate premature polymerization.

Digestion

15. If gelation was successful and a solid gel formed without empty spaces or air bubbles trapped in it, add 1 mL of digestion buffer (50 mM Tris pH 8.0, 1 mM

EDTA, 0.5% Triton X-100, 0.8 M guanidine HCl with the addition of 8 U/mL proteinase-K) to the sample and incubate overnight at room temperature.

Note: In case that the volume of the gelling solution is 200 μL, mix the 1.5 mL of digestion buffer with 0.5 mL of 8 U/mL proteinase-K. The volume of the gelling solution can vary depending on the gelling chamber or the dish where the gelation is going to occur. The volume of the digestion buffer must be at least 10 times larger than the volume of the gelling solution. If glutaraldehyde is used for anchoring, the digestion time should not exceed 1 h.

5.5.3 Day 3

Expansion with water

16. The next day, the gel has absorbed the water from the digestion buffer, has already doubled in size and is floating in the remaining digestion buffer. Immerse the gel into excess volume of ddH_2O for 20 min, four or five times exchanging the water in sequence of 20 min, until no further expansion of the gel can be visualized after successive water exchanges.

    Note: After expansion, the gel is visibly larger than in the beginning of the protocol, as shown in Fig. 1B.

17. Add 1 mL of the 100 nM solution of SiR–DNA or 1 mL of the 1 μg/mL solution of DAPI to the sample and incubate for 15–20 min for visualization of chromosomes in the sample

5.6 Protocol for expansion microscopy of PRC1-GFP

5.6.1 Day 1

Fixation

1. Fix the cells (we used HeLa-Kyoto BAC line stably expressing PRC1-GFP) with 1 mL of 100% methanol for 3 min at −20 °C.
2. Wash cells in 1 mL of 1% PBS buffer three times for 5 min each.
3. For visualization of chromosomes, see Section 5.5—Chromosome staining and quality control.

Anchoring

4. Same as Section 5.5—Anchoring.

    Note: After experimenting with two anchoring agents, Acryloyl-X and 0.25% glutaraldehyde, we concluded that the best option for anchoring is Acryloyl-X since it can preserve the fluorescent proteins signal after overnight proteinase-K digestion, which 0.25% glutaraldehyde could not.

5.6.2 Day 2

Gelation

5. Same as Section 5.5—Gelation.

Digestion

6. Same as Section 5.5—Digestion.

Note: When expanding fluorescent proteins, the digestion time can be the same as when the antibodies are used, but only if Acryloyl-X is used for anchoring. If glutaraldehyde is used for anchoring, the digestion time should not exceed 1 h.

5.6.3 Day 3

Expansion with water

7. Same as Section 5.5—Expansion with water.

5.7 Imaging

We imaged expanded samples directly in the dish. Before imaging, excess water was removed by pipetting and by placing filter paper in the corners of the dish to minimize drift of the gel during imaging. Drift still sometimes occurred and often it could be resolved by trying to maximally remove excess water or by imaging fewer planes, which makes the time of the imaging shorter. Also, after expansion the gel can be cut into smaller pieces, which are more practical regarding drift reduction, but it is important to maintain the right orientation of the gel with the cell layer facing down. Cells were imaged with Bruker Opterra Multipoint Scanning Confocal Microscope (Bruker, Middleton, WI, USA) (Buđa, Vukušić, & Tolić, 2017). The system was mounted on a Nikon Ti-E inverted microscope equipped with a Nikon CFI Plan Apo 100 ×/1.4 numerical aperture oil objective (Nikon, Tokyo, Japan). A 60 µm pinhole aperture was used and the xy-pixel size was 83 nm. For excitation of DAPI, GFP, mCherry and SiR fluorescence, a 405, 488, 561 and 647 nm diode laser line was used, respectively. The excitation light was separated from the emitted fluorescence by using Dichroic and Barrier Filter Set 405/488/561/640 nm (DAPI/eGFP/TRITC/Cy5) (Chroma, USA). Images were captured with an Evolve 512 Delta EMCCD Camera (Photometrics, Tucson, AZ, USA) using 350 ms exposure time with no binning performed. Line averaging was set to 8 for the channel in which tubulin or PRC1 were imaged, in other channels this feature was not used. A whole spindle z-stack was imaged, acquired at 30–60 focal planes for immunofluorescence and 60–120 for expanded samples separated by 0.5 µm with unidirectional xyz scan mode. The system was controlled with the Prairie View Imaging Software (Bruker).

6 Analysis and statistics

6.1 Determining the expansion factor

After performing the protocol from Section 5.5, images of expanded spindles are obtained in four phases of mitosis: prophase (Fig. 2, left), metaphase (Fig. 2, middle), anaphase (Fig. 2, right) and telophase (Fig. 3). The quality of the ExM protocol was assessed by comparing images of astral microtubule region from unexpanded and expanded samples (Fig. 4) because the improvement of the image resolution is best visualized on single microtubules, such as astrals.

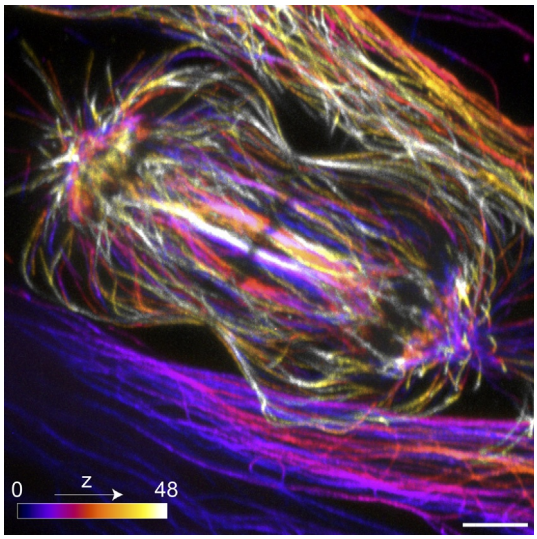

FIG. 3

Expansion microscopy of the telophase mitotic spindle. Maximum z-projection of a telophase RPE-1 cell and surrounding interphase cells stained with anti-alpha-tubulin and color coded through z-planes (from 0 to 48 μm) as described on the scheme (using ImageJ temporal color coding Lookup Table Fire). Scale bar, 5 μm.

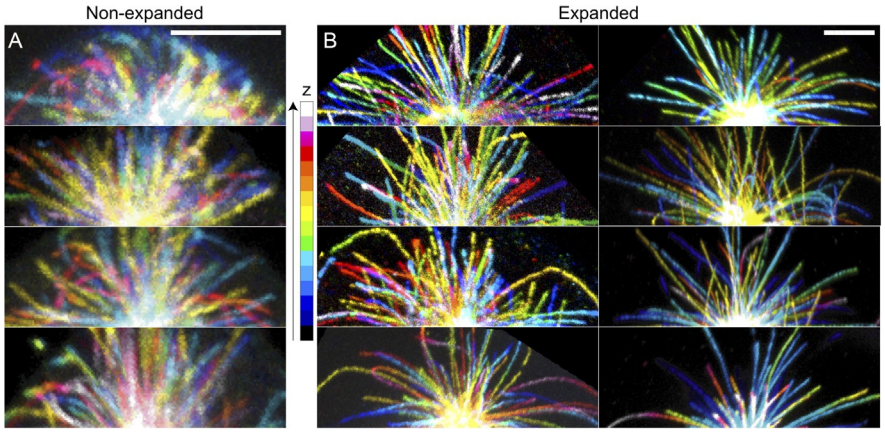

FIG. 4

Expansion microscopy yields better resolution of astral microtubules when compared to immunofluorescence only protocols. (A) Four examples of maximum z-projections of a region containing only astral microtubules in mitotic spindles of RPE-1 cells after immunofluorescence protocol using anti-alpha-tubulin antibody. Images are color-coded through z-planes as shown in the color bar on the right. (B) Eight examples of maximum z-projections of a region containing only astral microtubules in the mitotic spindles of RPE-1 cells stained with anti-alpha-tubulin after expansion microscopy. Images are color-coded through z-planes as shown in the color bar on the left (using ImageJ temporal color coding Lookup Table 16 colors). Scale bars, 5 μm.

Expansion factor is the ratio between one variable after expansion and the same variable before expansion and it shows how successful the expansion protocol was. In the past, three methods have been used to determine the expansion factor: measurement of the gel weight (Cipriano et al., 2014), measurement of the gel diameter (Cipriano et al., 2014), and determination by the microscopic analysis (Gao et al., 2017). The determination of the expansion factor by weight or the diameter of the gel is not precise because the gel is often not symmetrical and the excess water from the gel can never be fully removed. The most accurate method to estimate the expansion factor is by directly comparing pre-expanded and post-expanded biological samples. The approach is to acquire the overview image of the sample, preferably of the same structure before and after expansion, and then to rotate and scale the image to find the alignment in which the images could be compared. By using the distance measurement tools, the distance between clearly distinguishable landmarks can be measured. For most precise expansion factor estimation, it is recommended that the pre-expanded structure is the same one imaged after expansion. However, this could be challenging when the mitotic spindle is expanded since its size makes it difficult to later find the same spindle in the expanded gel, thus in our measurements, for the expansion factor estimation we used different spindles before and after expansion (Fig. 5). Comparing different spindles before and after expansion is not a problem because the length of the metaphase mitotic spindle is rather set in a

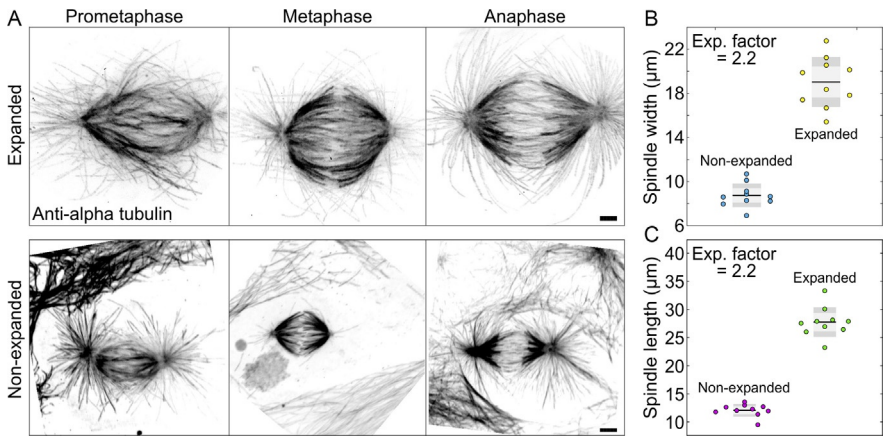

FIG. 5

Confocal fluorescence images of tubulin in the mitotic spindles, in different stages of mitosis, before and after expansion. (A) RPE-1 cells immunostained for anti-alpha tubulin, in prometaphase (left), metaphase (middle) and anaphase (right) before expansion (bottom) and after expansion (top). Top and bottom images do not represent the same cells. Images are the maximum projection of acquired z-stack. (B and C) Quantification (univariate scatter plot) of spindle widths (B) and lengths (C) before and after expansion. Boxes represent standard deviation (dark gray), 95% confidence interval of the mean (light gray) (light gray) and mean value (black). Scale bars, 5 µm.

population of cells (Goshima & Scholey, 2010). Here, the expansion factor was calculated as the ratio between the average length or width of the prometaphase and metaphase spindles before and after expansion (Fig. 5). The length of every mitotic spindle was measured as the distance between the centers of centrosomes. The width was measured as the distance between two outermost kinetochore-microtubule bundles on opposite sides of the spindle.

Mitotic spindles in prometaphase and metaphase were recognized by their shape and position of kinetochores and chromosomes and were imaged both pre-expansion, and post-expansion (Fig. 5A). Measurement was done on 10 spindles before expansion, 7 spindles from the RPE1 cell line, and 3 spindles from the U2OS cell line, and on 10 spindles after expansion, 9 spindles from the RPE1 cell line and 1 spindle from the U2OS cell line. There was no significant difference between the different cell lines.

Average length of the mitotic spindles before expansion was $12.49 \pm 0.3\,\mu m$ and the average width was $8.74 \pm 0.3\,\mu m$ (Fig. 5B and C). Average length of the mitotic spindles after expansion was $26.9 \pm 0.7\,\mu m$ and their average width was $19.03 \pm 0.6\,\mu m$ (Fig. 5B and C). Thus, the average expansion factor using this protocol was thus 2.15 ± 0.5 when comparing the length (Fig. 5C) and 2.21 ± 0.5 when calculated from width data (Fig. 5B). Expansion factor is smaller than expected when compared with the initial ExM protocol reporting expansion factor of 4 (Tillberg et al., 2016). This could be due to either problems with water purity, which could reduce the final expansion factor (Gao et al., 2017), or the spindle could specifically react to fixation by reducing both length and width resulting in the underestimation of the expansion factor. We should also note that we tried to adapt the X10 expansion microscopy protocol yielding higher expansion factors (Truckenbrodt et al., 2018), but we could not obtain sufficient tubulin signal in the spindle by using this protocol.

6.2 Comparison of approaches used to visualize the bridging fiber

We have recently shown that almost all interpolar microtubule bundles are associated with kinetochores and act as a bridge between sister kinetochore fibers (k-fibers) in metaphase, and were thus termed "bridging fibers" (Polak, Risteski, Lesjak, & Tolić, 2017). This fiber balances the tension between sister kinetochores in metaphase (Kajtez et al., 2016) and contributes to anaphase chromosome segregation (Vukušić et al., 2017). In our previous studies (Buđa et al., 2017; Kajtez et al., 2016; Polak et al., 2017), the number of microtubules in the bridging fiber was estimated from live cell images where tubulin was labeled either with GFP or mCherry fluorophore.

To compare various tubulin labeling approaches and differences between ExM, immunofluorescence and live imaging, we compared bridging fibers from various methods of tubulin visualization and their signal intensity profiles (Fig. 6). We found that the best method of bridging fiber visualization was ExM of anti-alpha tubulin fixed with 3.2% PFA and 0.25% GLA in PEM (Fig. 6A), followed by the immunofluorescence of anti-alpha tubulin fixed with the same fixatives (Fig. 6B).

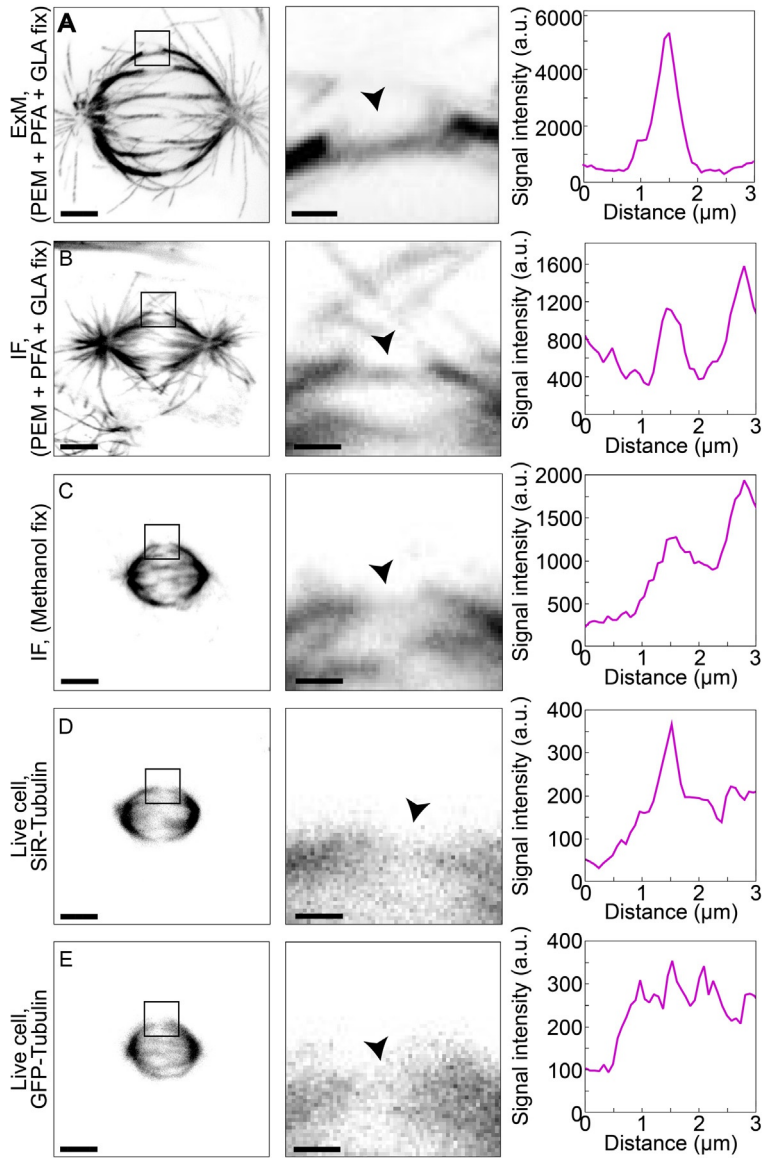

FIG. 6

Comparison of bridging fibers in confocal fluorescence images of the mitotic spindle, dyed with tubulin using different methods. (A–C) Expanded (ExM) and unexpanded immunofluorescence (IF) RPE-1 cells immunostained for anti-alpha tubulin, fixed (fix) with 3.2% paraformaldehyde and 0.25% glutaraldehyde in PEM buffer (A and B, left) or unexpanded RPE-1 cell fixed with 100% methanol (C, left). Each zoomed region indicates bridging fiber marked with an arrow (middle) and signal intensity profiles of the bridging fibers, taken perpendicular to the bridging fiber, from the images on the left (right). (D and E) Maximum projections of live RPE-1 cell dyed with 100 nM SiR-tubulin (D, left) or HeLa cell stably expressing tubulin-GFP (E, left), zoomed in bridging fiber region marked with arrow (middle) and signal intensity profile of the bridging fiber, taken perpendicular to the bridging fiber signal, from the images on the left (right). Note: bridging fiber peak signal is most evident on expanded sample. Scale bars, 5 μm (left panels) and 1 μm (middle panels).

Moderate quality of bridging fiber visualization was obtained in methanol fixed anti-alpha tubulin samples (Fig. 6C) and the lowest quality was obtained by live cell imaging of tubulin labeled with SiR-tubulin (Fig. 6D) or GFP-tubulin (Fig. 6E).

6.3 Estimation of the number of microtubules in the bridging fiber

To compare our ExM protocol with previous methods of estimation of bridging fiber thickness done on live cell images, we estimated the number of microtubules in the bridging fiber using the ExM images of anti-alpha tubulin by a method presented earlier (Fig. 7) (Buđa et al., 2017; Kajtez et al., 2016). In this analysis, the fluorescence signals of the bridging fibers and kinetochore fibers were measured and the ratios between them were used to calculate the relative number of microtubules in the bridging fiber compared to the kinetochore fiber. We measured the signal intensity of the microtubules between two sister kinetochores, I_b, and across the k-fiber near the kinetochore, I_{bk} (Fig. 7A and B). Fluorescence signal intensities were measured on 13 bridging and k-fibers in 7 different mitotic spindles, 6 from the RPE1 cell line and 1 from the U2OS cell line, from 5 independent experiments. As in Kajtez et al. (2016), the signal I_b was interpreted as the signal of the bridging fiber and I_{bk} as the sum of the k-fiber signal and the bridging fiber signal, $I_b + I_k$ (Fig. 7A). The ratio of the signal intensity of the microtubules between two sister kinetochores (I_b) and the signal of the k-fiber (I_{bk}), measured from the images of the expanded mitotic spindle in anti-alpha tubulin, is $42 \pm 3\%$ (Fig. 7C). From the obtained ratios, using

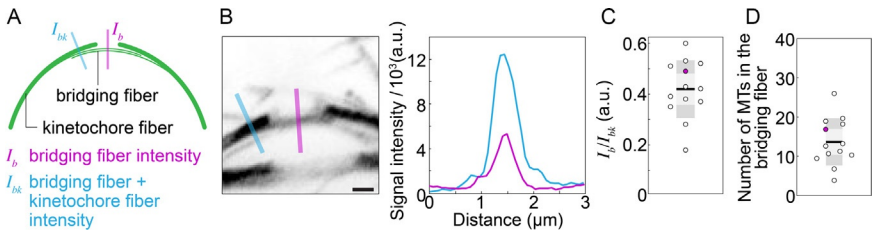

FIG. 7

Analysis of the number of microtubules in the bridging fiber. (A) Scheme showing the structure composed of sister k-fibers connected by the bridging fiber. Signal intensity of the bridging fiber, I_b, was measured along the magenta line, and for the bundle consisting of the bridging and the k-fiber, I_{bk}, along the blue line. (B) Zoomed region of expanded RPE1 cell, immunostained for anti-alpha tubulin, showing kinetochore and bridging fiber (left). Tubulin signal intensity of the bridging fiber, I_b (magenta, measured along the magenta line in the left image), and the bundle consisting of the bridging and the k-fiber, I_{bk} (blue, measured along the blue line), in the RPE1 cell from the left panel (right). (C and D) Quantification (univariate scatter plot) of I_b/I_{bk} ratio (C) and number of microtubules in the bridging fiber (D) from multiple RPE-1 cells. Boxes represent standard deviation (dark gray), 95% confidence interval of the mean (light gray), and the mean value (black). The magenta points correspond to the bridging fiber from panel (B). Scale bar, 1 μm.

$I_b/I_k = (I_b/I_{bk})/(1 - I_b/I_{bk})$ formula, we calculated I_b/I_k ratios and their mean value is $78 \pm 9\%$. From that we estimated that the bridging fiber contains $78 \pm 9\%$ of the number of microtubules in the k-fiber. Number of microtubules in the k-fiber from the electron micrographs was found to be around 17.5 (Wendell, Wilson, & Jordan, 1993). Accordingly, the number of microtubules in the bridging fiber is 13.7 ± 1.7 (Fig. 7D), when estimated from the expanded mitotic spindle images. This result corresponds well to the previously published results obtained from live mitotic spindles labeled with GFP-tubulin, which is 14 ± 2 microtubules in the bridging fiber (Kajtez et al., 2016).

6.4 Microtubule bundles in the mitotic spindle can be better resolved after expansion

In a population of mitotic cells in a dish, most of the mitotic spindles are horizontally oriented, in a way that the spindle long axis is parallel to the surface (Pietro, Echard, & Morin, 2016), as seen on 3D view of expanded metaphase mitotic spindle (Fig. 8A). However, we can also image vertically oriented spindles that can sometimes be found in a population of dividing cells. In these spindles, optical sections are

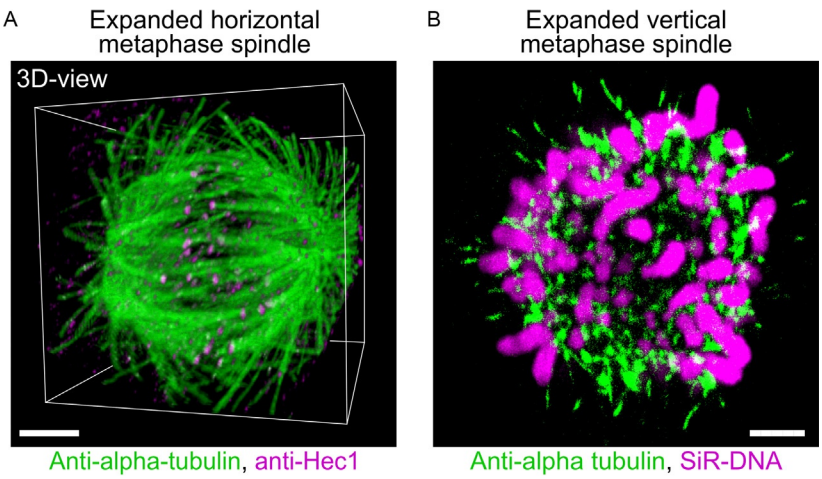

FIG. 8

Different views of expanded mitotic spindles depending on the orientation of the spindle in respect to the substrate. (A) 3D view of expanded RPE-1 horizontally oriented metaphase cell immunostained for anti-alpha tubulin (green) and anti-Hec1 (magenta) obtained using 3D Viewer plugin of ImageJ (voxel depth: 0.405, calculated by multiplying z-step size by a correction factor of 0.81, calculated in Novak et al. (2018); displayed as volume; resampling factor: 2.5). (B) Maximum z-projection of middle planes of vertically oriented RPE-1 cell immunostained for anti-alpha tubulin (green) and labeled with 100 nM SiR-DNA (magenta) in metaphase. Scale bar, 5 μm.

roughly perpendicular to the microtubule bundles which allows for precise localization of the microtubule bundles in each cross-section (Novak et al., 2018), as seen on expanded vertical metaphase spindle (Fig. 8B).

As vertically oriented spindles are rarely present in the sample, it is possible to transform horizontally oriented spindles into vertical view (pole-to-pole) by using a code written in R programming language (Novak et al., 2018). For this analysis, only the spindles with both poles roughly in the same plane were used to ensure that spindles were maximally vertical after the transformation into vertical orientation. Before the transformation, the z-stack of the spindle in a single channel was rotated in Fiji so that the spindle major axis was approximately parallel to the x-axis. Signal intensity at each pixel in a z-stack is denoted as $I(i, j, k)$, where indices i, j denotes coordinates in the imaging plane, and k denotes the number of the imaging plane of the z-stack. To transform the 3D image of the spindle into vertical orientation, we applied the transformation $I'(i, j, k) = I(k, i, j)$, which preserves the orientation of the coordinate system, that is, corresponds to rotation of the image without mirroring. The coordinates (i, j, k) correspond to 3D positions $(x, y, z) = (i \cdot \text{pixel size}, j \cdot \text{pixel size}, k \cdot z\text{-distance})$. The aberrations caused by refractive index mismatch between immersion oil and aqueous sample were considered by multiplying z-step size by a correction factor of 0.81 to obtain the correct z-distance (Novak et al., 2018).

As seen on Fig. 9, there is a clear improvement of resolution of horizontally oriented spindles when comparing their images before and after expansion (Fig. 9A and B). This improvement is also visible in the vertical view (equatorial plane) of the same spindles (Fig. 9C and D). The maximum expected number of microtubule bundles in the equatorial plane of a metaphase spindle in non-transformed human cell lines is close to the number of chromosomes, 46. This is because each chromosome is attached to k-fibers extending toward the opposite spindle poles and a bridging fiber connecting the k-fibers (see Fig. 7A) (Polak et al., 2017). In the equatorial plane, we usually see a cross-section of the bridging fiber if the chromosome is aligned at the metaphase plate, or a cross-section of a k-fiber if the chromosome is not perfectly aligned. Therefore, one microtubule bundle per chromosome is expected to cross the equatorial plane. The number of microtubule bundles that we counted in the equatorial plane (in the vertical view) of the RPE1 spindle before expansion was 22 while the same parameter after expansion in the same cell line was 40, close to the maximum expected number. Thus, the number of microtubule bundles that could be discerned in the vertical view before expansion is two times smaller than in the expanded sample (Fig. 9C and D). The diameter of the single microtubule bundle before expansion was $1.41 \pm 0.06\,\mu\text{m}$ ($n = 20$), and after expansion the diameter was $3.45 \pm 0.09\,\mu\text{m}$ ($n = 40$).

6.5 PRC1-GFP on microtubule bundles in expanded spindles

Since expansion of the GFP-tagged proteins was proven to be possible (Chozinski et al., 2016; Tillberg et al., 2016), this means that any protein tagged with the appropriate fluorophore could be expanded. However, we encountered problems when

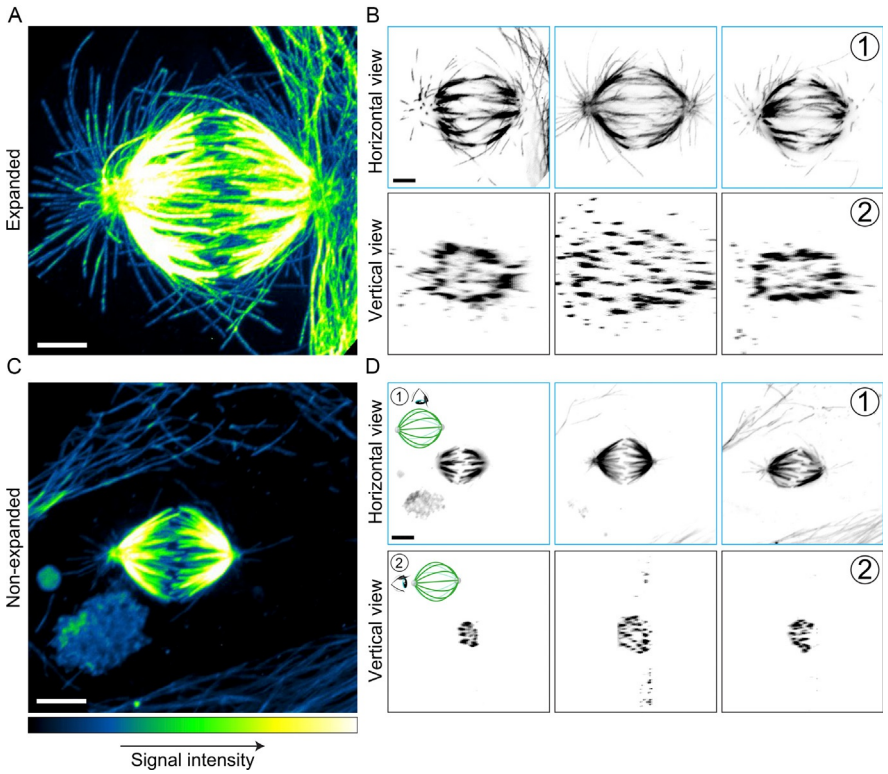

FIG. 9

Expansion microscopy of mitotic spindle in both horizontal and vertical views yields better resolution of microtubule bundles. (A and B) Expanded (A) and non-expanded (B) RPE-1 cells in a horizontal view, shown in maximum z-projections, immunostained for anti-alpha tubulin. Signal intensity level is color coded as specified on the bottom using ImageJ Lookup Table Green Fire Blue. (C) Individual z-planes of the cell from (A) viewed along spindle horizontal axis (indicated with 1) (top) and individual z-planes of the cells from (A) after transformation into vertical, pole-to-pole view (indicated with 2) (bottom). (D) Individual z-planes of the cell from (B) viewed along spindle horizontal axis (indicated with 1), as shown on the scheme (top) and individual z-planes of the cells from (B) after transformation into vertical, pole-to-pole view (indicated with 2), as shown on the scheme (bottom). Note: more microtubule bundles could be discerned in both horizontal and vertical views of the mitotic spindle after expansion microscopy. Scale bars, 5 μm.

trying to use this protocol to expand the microtubule-associated proteins because low expression levels of some GFP-tagged proteins led to highly disrupted signal after digestion. Thus, digestion times, especially if using GLA as anchoring agent, must be optimized to match specific protein of interest in a way that the digestion time should not exceed 1 h in this situation.

We imaged PRC1, a nuclear protein in interphase, that becomes associated with mitotic spindles in a highly dynamic manner during early mitosis, and later localizes to the cell midbody during cytokinesis in a highly clustered manner (Jiang et al., 1998). PRC1 is a microtubule-associated protein required to maintain the spindle midzone in late anaphase (Mollinari et al., 2002) and it binds to antiparallel overlap regions of the bridging microtubules in the metaphase spindle (Kajtez et al., 2016). Fig. 10 shows images of mitotic spindles labeled with PRC1-GFP before and after expansion in metaphase and telophase following protocol from Section 5.6. Even though the expansion is clearly visible when compared to mitotic spindles before expansion both in metaphase (Fig. 10A, left) and telophase (Fig. 10B, left), loss of fluorescence signal is noticeable in expanded spindles (Fig. 10A and B, right), especially in metaphase where PRC1 protein is more dynamic in comparison to telophase spindles (Pamula et al., 2019). Overall, more PRC1-labeled antiparallel MT bundles could be discerned in expanded than in non-expanded images in the same phase of mitosis (Fig. 10A and B). Accordingly, by using 100% cold-methanol fixation, anchoring exclusively with AcX molecule, or drastically reducing digestion times by ProK if using GLA anchoring (see Section 5.6), this protocol could be used to expand samples with any GFP-tagged microtubule-associated protein. However, signal of some fluorescently tagged proteins can greatly diminish, like shown for PRC1, restricting usage of such protocols to specific clustered microtubule-associated proteins, such as the centrosome-localized Kif25 protein (Decarreau et al., 2017).

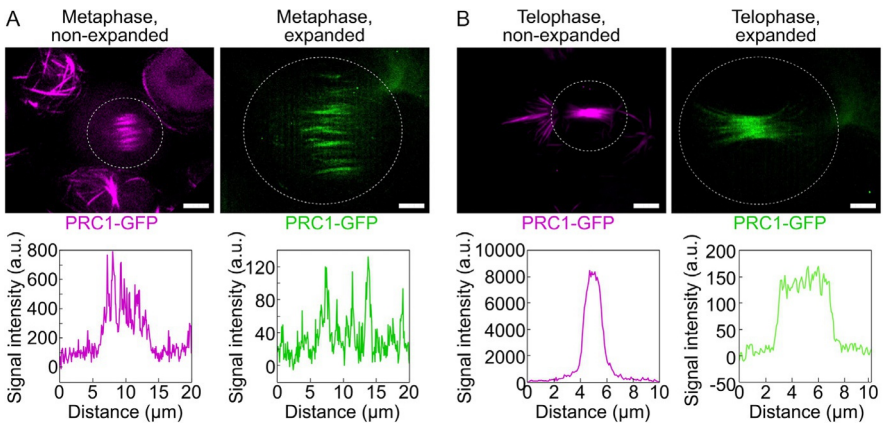

FIG. 10

Expansion microscopy of PRC1 protein tagged with GFP enables better resolution of antiparallel microtubule bundles. (A and B) Maximum projection of live HeLa metaphase (A) and telophase (B) cells stably expressing PRC1-GFP before (left, magenta) and different cells in the same stage after expansion (right, green). Signal intensity profile of the PRC1-GFP signal taken perpendicular to spindle long axis is shown in both conditions (bottom). Note: more PRC1-labeled bundles are distinguished after expansion. Scale bar, 5 μm.

7 Summary

Here, we presented a 3-day expansion microscopy protocol for tubulin staining in the mitotic spindle. The protocol was simplified in comparison with most current protocols in a way that staining, gelation, digestion and expansion steps are done directly in the dish in which cells are seeded so there is no need for special equipment. The basis of this method is the immunofluorescence protocol optimized specifically for the tubulin in the mitotic spindle, where the resolution is then improved with the addition of the expansion steps. The developed protocol, with relatively simple alterations in fixation and digestion steps, could be used for expansion of every protein in the mitotic spindle, after performing optimization steps. For example, PRC1-GFP protein in the spindle can be expanded by using 100% methanol as fixative instead PFA/GLA combination, by considerably reducing the ProK digestion time if using GLA for anchoring or by using exclusively AcX for anchoring.

In addition, we presented different uses of expansion microscopy for study of specific questions related to the mitotic spindle. Primarily, this protocol can be used to re-evaluate past results which were possibly a product of less precise and often distorted immunofluorescence images, yielding imprecise results. Also, transforming the view on the expanded mitotic spindles from horizontal to vertical could bring new insights into the complete, three-dimensional contour of the microtubule bundles, now in super-resolution. In the future, the combination of presented expansion microscopy protocol with other super-resolution methods could offer a powerful tool for the investigation of the complexity of mitotic spindle architecture and function.

Acknowledgments

The authors thank Renata Buđa for help in development of this protocol; Marin Barišić and Helder Maiato for U2OS cell line, Alexey Khodjakov for RPE1 cell line and Ina Poser and Tony Hyman for HeLa-Kyoto BAC line; Juraj Simunić and all other members of Tolić group for helpful discussions and advices regarding experimental design for ExM experiments; and Ivana Šarić for help with figures. This work was funded by the European Research Council (ERC Consolidator Grant, GA number 647077), Croatian Science Foundation (Project IP-2014-09-4753), Croatian Science Foundation Cooperation Programme with Croatian Scientists in Diaspora "Research Cooperability" (Project PZS-2019-02-7653), QuantiXLie Centre of Excellence, a project cofinanced by the Croatian Government and European Union through the European Regional Development Fund - the Competitiveness and Cohesion Operational Programme (Grant KK.01.1.1.01.0004) and the Science and Innovation Grant cofinanced by the European Structural and Investment Funds (ESIF) within the Operational Programme Competitiveness and Cohesion (OPCC) 2014–2020 (Grant KK.01.1.1.04.0057).

References

Asano, S. M., Gao, R., Wassie, A. T., Tillberg, P. W., Chen, F., & Boyden, E. S. (2018). Expansion microscopy: Protocols for imaging proteins and RNA in cells and tissues. *Current Protocols in Cell Biology, 80*(1), e56. https://doi.org/10.1002/cpcb.56.

Betzig, E., Patterson, G. H., Sougrat, R., Lindwasser, O. W., Olenych, S., Bonifacino, J. S., et al. (2006). Imaging intracellular fluorescent proteins at nanometer resolution. *Science*, *313*(5793), 1642–1645. https://doi.org/10.1126/science.1127344.

Born, M., Wolf, E., Bhatia, A. B., Clemmow, P. C., Gabor, D., Stokes, A. R., et al. (1999). *Elements of the theory of diffraction.* In Principles of Optics. Cambridge: Cambridge University Press. https://doi.org/10.1017/cbo9781139644181.

Buđa, R., Vukušić, K., & Tolić, I. M. (2017). Dissection and characterization of microtubule bundles in the mitotic spindle using femtosecond laser ablation. *Methods in Cell Biology*, *139*, 81–101. https://doi.org/10.1016/bs.mcb.2016.11.007.

Busson, S., Dujardin, D., Moreau, A., Dompierre, J., & De Mey, J. R. (1998). Dynein and dynactin are localized to astral microtubules and at cortical sites in mitotic epithelial cells. *Current Biology*, *8*(9), 541–544. https://doi.org/10.1016/S0960-9822(98)70208-8.

Chang, J. B., Chen, F., Yoon, Y. G., Jung, E. E., Babcock, H., Kang, J. S., et al. (2017). Iterative expansion microscopy. *Nature Methods*, *14*(6), 593–599. https://doi.org/10.1038/nmeth.4261.

Chen, F., Tillberg, P. W., & Boyden, E. S. (2015). Expansion microscopy. *Science*, *347*(6221), 543–548. https://doi.org/10.1126/science.1260088.

Chen, F., Wassie, A. T., Cote, A. J., Sinha, A., Alon, S., Asano, S., et al. (2016). Nanoscale imaging of RNA with expansion microscopy. *Nature Methods*, *13*(8), 679–684. https://doi.org/10.1038/nmeth.3899.

Chozinski, T. J., Halpern, A. R., Okawa, H., Kim, H. J., Tremel, G. J., Wong, R. O. L., et al. (2016). Expansion microscopy with conventional antibodies and fluorescent proteins. *Nature Methods*, *13*(6), 485–488. https://doi.org/10.1038/nmeth.3833.

Cipriano, B. H., Banik, S. J., Sharma, R., Rumore, D., Hwang, W., Briber, R. M., et al. (2014). Superabsorbent hydrogels that are robust and highly stretchable. *Macromolecules*, *47*(13), 4445–4452. https://doi.org/10.1021/ma500882n.

Coelho, M., Maghelli, N., & Tolić-Nørrelykke, I. M. (2013). Single-molecule imaging in vivo: The dancing building blocks of the cell. *Integrative Biology (United Kingdom)*, *5*, 748–758. https://doi.org/10.1039/c3ib40018b.

Decarreau, J., Wagenbach, M., Lynch, E., Halpern, A. R., Vaughan, J. C., Kollman, J., et al. (2017). The tetrameric kinesin Kif25 suppresses pre-mitotic centrosome separation to establish proper spindle orientation. *Nature Cell Biology*, *19*(4), 384–390. https://doi.org/10.1038/ncb3486.

Forth, S., & Kapoor, T. M. (2017). The mechanics of microtubule networks in cell division. *Journal of Cell Biology*, *216*, 1525–1531. https://doi.org/10.1083/jcb.201612064.

Freifeld, L., Odstrcil, I., Förster, D., Ramirez, A., Gagnon, J. A., Randlett, O., et al. (2017). Expansion microscopy of zebrafish for neuroscience and developmental biology studies. *Proceedings of the National Academy of Sciences of the United States of America*, *114*(50), E10799–E10808. https://doi.org/10.1073/pnas.1706281114.

Gambarotto, D., Zwettler, F. U., Le Guennec, M., Schmidt-Cernohorska, M., Fortun, D., Borgers, S., et al. (2019). Imaging cellular ultrastructures using expansion microscopy (U-ExM). *Nature Methods*, *16*(1), 71–74. https://doi.org/10.1038/s41592-018-0238-1.

Gao, R., Asano, S. M., & Boyden, E. S. (2017). Q & A: Expansion microscopy. *BMC Biology*, *15*(1), 50. https://doi.org/10.1186/s12915-017-0393-3.

Gao, M., Maraspini, R., Beutel, O., Zehtabian, A., Eickholt, B., Honigmann, A., et al. (2018). Expansion stimulated emission depletion microscopy (ExSTED). *ACS Nano*, *12*(5), 4178–4185. https://doi.org/10.1021/acsnano.8b00776.

Geertsema, H., & Ewers, H. (2016). Expansion microscopy passes its first test. *Nature Methods*, *13*, 481–482. https://doi.org/10.1038/nmeth.3872.

Goshima, G., & Scholey, J. M. (2010). Control of mitotic spindle length. *Annual Review of Cell and Developmental Biology*, *26*(1), 21–57. https://doi.org/10.1146/annurev-cellbio-100109-104006.

Gustafsson, M. G. L. (2000). Surpassing the lateral resolution limit by a factor of two using structured illumination microscopy. *Journal of Microscopy*, *198*(2), 82–87. https://doi.org/10.1046/j.1365-2818.2000.00710.x.

Hendry, J. H., & Scott, D. (1987). Loss of reproductive integrity of irradiated cells, and its importance in tissues. In C. S. Potten (Ed.), *Perspectives on mammalian cell death* (p. 160). Oxford: Oxford Scientific Publications. https://doi.org/10.1016/0092-8674(88)90084-0.

Jiang, W., Jimenez, G., Wells, N. J., Hope, T. J., Wahl, G. M., Hunter, T., et al. (1998). PRC1: A human mitotic spindle-associated CDK substrate protein required for cytokinesis. *Molecular Cell*, *2*(6), 877–885. https://doi.org/10.1016/s1097-2765(00)80302-0.

Kajtez, J., Solomatina, A., Novak, M., Polak, B., Vukušić, K., Rüdiger, J., et al. (2016). Overlap microtubules link sister k-fibres and balance the forces on bi-oriented kinetochores. *Nature Communications*, *7*(1), 1–11. https://doi.org/10.1038/ncomms10298.

Kisselev, A. F., & Goldberg, A. L. (2001). Proteasome inhibitors: From research tools to drug candidates. *Chemistry and Biology*, *8*, 739–758. https://doi.org/10.1016/S1074-5521(01)00056-4.

Klar, T. A., Jakobs, S., Dyba, M., Egner, A., & Hell, S. W. (2000). Fluorescence microscopy with diffraction resolution barrier broken by stimulated emission. *Proceedings of the National Academy of Sciences of the United States of America*, *97*(15), 8206–8210. https://doi.org/10.1073/pnas.97.15.8206.

Ku, T., Swaney, J., Park, J. Y., Albanese, A., Murray, E., Hun Cho, J., et al. (2016). Multiplexed and scalable super-resolution imaging of three-dimensional protein localization in size-adjustable tissues. *Nature Biotechnology*, *34*(9), 973–981. https://doi.org/10.1038/nbt.3641.

Maiato, H., Gomes, A. M., Sousa, F., & Barisic, M. (2017). Mechanisms of chromosome congression during mitosis. *Biology, 6*(1). https://doi.org/10.3390/biology6010013.

Mollinari, C., Kleman, J. P., Jiang, W., Schoehn, G., Hunter, T., & Margolis, R. L. (2002). PRC1 is a microtubule binding and bundling protein essential to maintain the mitotic spindle midzone. *Journal of Cell Biology*, *157*(7), 1175–1186. https://doi.org/10.1083/jcb.200111052.

Novak, M., Polak, B., Simunić, J., Boban, Z., Kuzmić, B., Thomae, A. W., et al. (2018). The mitotic spindle is chiral due to torques within microtubule bundles. *Nature Communications, 9*(1). https://doi.org/10.1038/s41467-018-06005-7.

Pamula, M. C., Carlini, L., Forth, S., Verma, P., Suresh, S., Legant, W. R., et al. (2019). High-resolution imaging reveals how the spindle midzone impacts chromosome movement. *The Journal of Cell Biology*, *218*(8), 2529–2544. https://doi.org/10.1083/jcb.201904169.

Pavin, N., & Tolić, I. M. (2016). Self-organization and forces in the mitotic spindle. *Annual Review of Biophysics*, *45*, 279–298. https://doi.org/10.1146/annurev-biophys-062215-010934.

Pietro, F., Echard, A., & Morin, X. (2016). Regulation of mitotic spindle orientation: An integrated view. *EMBO Reports*, *17*(8), 1106–1130. https://doi.org/10.15252/embr.201642292.

Polak, B., Risteski, P., Lesjak, S., & Tolić, I. M. (2017). PRC1-labeled microtubule bundles and kinetochore pairs show one-to-one association in metaphase. *EMBO Reports*, *18*(2), 217–230. https://doi.org/10.15252/embr.201642650.

Prosser, S. L., & Pelletier, L. (2017). Mitotic spindle assembly in animal cells: A fine balancing act. *Nature Reviews Molecular Cell Biology*, *18*, 187–201. https://doi.org/10.1038/nrm.2016.162.

Rust, M. J., Bates, M., & Zhuang, X. (2006). Sub-diffraction-limit imaging by stochastic optical reconstruction microscopy (STORM). *Nature Methods*, *3*(10), 793–795. https://doi.org/10.1038/nmeth929.

Sacristan, C., Ahmad, M. U. D., Keller, J., Fermie, J., Groenewold, V., Tromer, E., et al. (2018). Dynamic kinetochore size regulation promotes microtubule capture and chromosome biorientation in mitosis. *Nature Cell Biology*, *20*(7), 800–810. https://doi.org/10.1038/s41556-018-0130-3.

Schnell, U., Dijk, F., Sjollema, K. A., & Giepmans, B. N. G. (2012). Immunolabeling artifacts and the need for live-cell imaging. *Nature Methods*, *9*, 152–158. https://doi.org/10.1038/nmeth.1855.

So, C., Seres, K. B., Steyer, A. M., Mönnich, E., Clift, D., Pejkovska, A., et al. (2019). A liquid-like spindle domain promotes acentrosomal spindle assembly in mammalian oocytes. *Science, 364*(6447). https://doi.org/10.1126/science.aat9557.

Thorley, J. A., Pike, J., & Rappoport, J. Z. (2014). Super-resolution microscopy: A comparison of commercially available options. In A. Cornea & P. M. Conn (Eds.), *Fluorescence microscopy*. Elsevier. https://doi.org/10.1016/B978-0-12-409513-7.00014-2.

Thornton, B. R., & Toczyski, D. P. (2003). Securin and B-cyclin/CDK are the only essential targets of the APC. *Nature Cell Biology*, *5*(12), 1090–1094. https://doi.org/10.1038/ncb1066.

Tillberg, P. W., Chen, F., Piatkevich, K. D., Zhao, Y., Yu, C. C., English, B. P., et al. (2016). Protein-retention expansion microscopy of cells and tissues labeled using standard fluorescent proteins and antibodies. *Nature Biotechnology*, *34*(9), 987–992. https://doi.org/10.1038/nbt.3625.

Truckenbrodt, S., Maidorn, M., Crzan, D., Wildhagen, H., Kabatas, S., & Rizzoli, S. O. (2018). X10 expansion microscopy enables 25-nm resolution on conventional microscopes. *EMBO Reports, 19*(9). https://doi.org/10.15252/embr.201845836.

Truckenbrodt, S., Sommer, C., Rizzoli, S. O., & Danzl, J. G. (2019). A practical guide to optimization in X10 expansion microscopy. *Nature Protocols*, *14*(3), 832–863. https://doi.org/10.1038/s41596-018-0117-3.

Vassilev, L. T., Tovar, C., Chen, S., Knezevic, D., Zhao, X., Sun, H., et al. (2006). Selective small-molecule inhibitor reveals critical mitotic functions of human CDK1. *Proceedings of the National Academy of Sciences of the United States of America*, *103*(28), 10660–10665. https://doi.org/10.1073/pnas.0600447103.

Vukušić, K., Buđa, R., Bosilj, A., Milas, A., Pavin, N., & Tolić, I. M. (2017). Microtubule sliding within the bridging fiber pushes kinetochore fibers apart to segregate chromosomes. *Developmental Cell*, *43*(1), 11–23.e6. https://doi.org/10.1016/j.devcel.2017.09.010.

Vukušić, K., Buđa, R., & Tolić, I. M. (2019). Force-generating mechanisms of anaphase in human cells. *Journal of Cell Science, 132*. https://doi.org/10.1242/jcs.231985.

Wang, Y., Yu, Z., Cahoon, C. K., Parmely, T., Thomas, N., Unruh, J. R., et al. (2018). Combined expansion microscopy with structured illumination microscopy for analyzing protein complexes. *Nature Protocols*, *13*(8), 1869–1895. https://doi.org/10.1038/s41596-018-0023-8.

Wassie, A. T., Zhao, Y., & Boyden, E. S. (2019). Expansion microscopy: Principles and uses in biological research. *Nature Methods*, *16*, 33–41. https://doi.org/10.1038/s41592-018-0219-4.

Wendell, K. L., Wilson, L., & Jordan, M. A. (1993). Mitotic block in HeLa cells by vinblastine: Ultrastructural changes in kinetochore-mcirotubule attachment and in centrosomes. *Journal of Cell Science*, *104*(2), 261–274.

Zhang, Y. S., Chang, J. B., Alvarez, M. M., Trujillo-De Santiago, G., Aleman, J., Batzaya, B., et al. (2016). Hybrid microscopy: Enabling inexpensive high-performance imaging through combined physical and optical magnifications. *Scientific Reports, 6*. https://doi.org/10.1038/srep22691.

Zhao, Y., Bucur, O., Irshad, H., Chen, F., Weins, A., Stancu, A. L., et al. (2017). Nanoscale imaging of clinical specimens using pathology-optimized expansion microscopy. *Nature Biotechnology*, *35*(8), 757–764. https://doi.org/10.1038/nbt.3892.